Investigation of the Influence of Hydrofluoric Acid and Temperature on the Sintering Processes and Phase Formation in Alumina Nanofiber-based Ceramics

Alex S. Demianov
Federal Research Center "Krasnoyarsk Science Center of the Siberian Branch of the Russian Academy of Sciences", Russian Academy of Sciences (FRC KSC SB RAS), Krasnoyarsk, Russia | Siberian Federal University, Krasnoyarsk, Russia
lex-demyan@mail.ru

Sergey S. Dobrosmyslov
Federal Research Center "Krasnoyarsk Science Center of the Siberian Branch of the Russian Academy of Sciences", Russian Academy of Sciences (FRC KSC SB RAS), Krasnoyarsk, Russia | Siberian Federal University, Krasnoyarsk, Russia
dobrosmislov.s.s@gmail.com (corresponding author)

Gennady E. Nagibin
Federal Research Center "Krasnoyarsk Science Center of the Siberian Branch of the Russian Academy of Sciences", Russian Academy of Sciences (FRC KSC SB RAS), Krasnoyarsk, Russia | Siberian Federal University, Krasnoyarsk, Russia
nagibin1@gmail.com

Anton S. Voronin
Federal Research Center "Krasnoyarsk Science Center of the Siberian Branch of the Russian Academy of Sciences", Russian Academy of Sciences (FRC KSC SB RAS), Krasnoyarsk, Russia | Siberian Federal University, Krasnoyarsk, Russia
a.voronin1988@mail.ru

Mihail M. Simunin
Federal Research Center "Krasnoyarsk Science Center of the Siberian Branch of the Russian Academy of Sciences", Russian Academy of Sciences (FRC KSC SB RAS), Krasnoyarsk, Russia | Siberian Federal University, Krasnoyarsk, Russia
michanel@mail.ru

Airana A. Kyylar
Federal Research Center "Krasnoyarsk Science Center of the Siberian Branch of the Russian Academy of Sciences", Russian Academy of Sciences (FRC KSC SB RAS), Krasnoyarsk, Russia
ayraana.kuular@mail.ru

Maksim S. Molokeev
Laboratory of Crystal Physics, Kirensky Institute of Physics, Federal Research Center (KSC SB RAS), Krasnoyarsk, Russia | Department of Physics, Far Eastern State Transport University, Khabarovsk, Russia
msmolokeev@mail.ru

Elena N. Fedorova
Siberian Federal University, Krasnoyarsk, Russia
fedorova.elena.85@gmail.com

Marina A. Perkova
Siberian Federal University, Krasnoyarsk, Russia
dero-gai@mail.ru

Ivan V. Nemtsev
Federal Research Center "Krasnoyarsk Science Center of the Siberian Branch of the Russian Academy of Sciences", Russian Academy of Sciences (FRC KSC SB RAS), Krasnoyarsk, Russia| Kirensky Institute of Physics, Federal Research Center (KSC SB RAS), Krasnoyarsk, Russia | Siberian Federal University, Krasnoyarsk, Russia
ivan_nemtsev@mail.ru

Stanislav V. Khartov
Federal Research Center "Krasnoyarsk Science Center of the Siberian Branch of the Russian Academy of Sciences", Russian Academy of Sciences (FRC KSC SB RAS), Krasnoyarsk, Russia
stas_f1@list.ru

Received: 11 November 2024 | Revised: 5 December 2024 | Accepted: 8 December 2024

 DOI: https://doi.org/10.48084/etasr.9547

ABSTRACT

This work studies a ceramic material, synthesized from alumina nanofiber via semi-dry pressing with an average diameter of 10 nm and a high aspect ratio (>1000), with Hydrofluoric Acid (HF) used as a mineralizer. The effects of varying firing temperature and HF concentration were systematically investigated. The material was characterized using electron microscopy, X-ray fluorescence analysis, and X-ray phase analysis, while thermodynamic calculations of phase transformations were conducted. Additionally, strength, density, and open porosity were analyzed as functions of the processing parameters. The analysis revealed that an optimal HF concentration of 1% and a firing temperature of 800 °C yield the best physical and mechanical properties. Furthermore, the transition mechanism from the γ-phase to the α-phase under varying HF concentrations and firing temperatures was examined. A linear dependence of the concentration of Fluorine (F) atoms in the ceramic material on the firing temperature was established. The maximum physical and mechanical characteristics include a compressive strength of 49 MPa with a porosity of 46% and a density of 1.47 g/cm³.

Keywords-ceramics; nanofiber; aluminum oxide; hydrofluoric acid; microstructure; compressive strength

I. INTRODUCTION

Fibrous ceramics are useful materials for various industries due to their unique properties, including high heat resistance [1], mechanical strength [2, 3], chemical resistance [4, 5], low density [6, 7], flexibility [8, 9], and good electrical insulation [10]. These properties enable their application in diverse industrial sectors, such as construction [11], aerospace [12, 13], energy [14], and metallurgy [15]. In the aerospace industry, fibrous ceramics are used to create heat-protective coatings and components that can withstand extreme temperatures and mechanical loads [16]. In the energy industry, they are used in thermal insulation and structures operating in aggressive environments, such as gas turbines and furnaces [17]. In metallurgy, they are utilized to manufacture filters and components resistant to the corrosive effects of molten metals [18]. The primary unique characteristic of fibrous ceramics is their excellent filtering properties [19-21], provided by high porosity and increased surface area [22]. These characteristics allow efficient particle retention with minimal flow resistance while maintaining resistance to chemically aggressive conditions. They are also easily regenerated and tailored to specific filtration applications [23, 24]. γ-Al2O3, a form of aluminum oxide, possesses high porosity, significant specific surface area, high catalytic activity, and considerable thermal stability [25, 26]. In industry, γ-Al2O3 is used as an adsorbent, catalyst, and catalyst carrier in petrochemistry [27-29] and ecology [30]. As an adsorbent and catalyst, γ-Al_2O_3 is effectively employed in purification and catalysis processes [31, 32]. It is also deployed in air and water purification systems due to its ability to adsorb pollutants. Research in the field of γ-Al2O3 synthesis continues, with an emphasis on improving its physical and chemical properties for wider application in industrial sectors. Researchers at the Federal Research Center KSC SB RAS have developed a method for producing nano-sized γ-Al_2O_3 nanofibers by directed oxidation of aluminum from a melt [33]. This technique allows the

formation of nanoscale fibers with a diameter of 5-50 nm and a length of about 1 cm, forming an intertwined bundle. These fibers are characterized by unique properties, such as a small diameter and a high aspect ratio (>1000), which surpass existing analogs [34]. HF can destroy the structure of alumina ceramics, causing chemical etching of the surface. This effect leads to a decrease in the activation energy of the γ-to-α phase transition, as well as an intensification of ceramic processes. Consequently, HF can act as a mineralizer for alumina, which leads to a decrease in sintering temperature, improved mechanical properties, and increased homogeneity of the microstructure, thereby enhancing the performance characteristics of ceramic products [35]. Modern materials, such as γ-Al_2O_3 fibrous ceramics, play a key role in the development of technologies due to their unique properties and their ability to adapt to the specific requirements of various industries.

The main objective of this work is to study the influence of HF on the sintering and phase formation process in a ceramic material obtained from a fibrous batch with a high aspect ratio of γ-Al_2O_3.

II. MATERIALS AND EQUIPMENT

The nanofibers were synthesized using the directed oxidation of aluminum from a melt [33]. This technique enables the production of nanosized fibers with a diameter ranging from 5 to 50 nm and a length of approximately 1 cm, thereby forming an intertwined bundle of fibers, as depicted in Figure 1. To activate the sintering process, HF of analytical grade was used as a mineralizer. Before use, the fiber was crushed in a mortar and then treated with a solution of HF at various concentrations (1%, 2%, and 3%) in a weight ratio of 1:1. After treatment, the material was dried at a temperature of 110 °C until no further weight loss was observed. The material was then mixed with a 3% solution of polyvinyl alcohol (PVA) in a ratio of 10:1. Samples with a diameter of 12 mm and a height of 10 mm were produced using the semi-dry pressing method [36]. Pressing was carried out on a hydraulic press IP-100. After production, the samples were subjected to controlled heating at a rate of 5 °C/min, with a holding time of 120 minutes at the target temperature. The samples were heated in a high-temperature electric furnace in air (PVK-1.6-12) in a temperature range of 100 °C to 1600 °C, with a working area volume of 12 L. Firing was carried out at temperatures of 700 °C, 800 °C, 900 °C, and 1000 °C. After manufacturing, the compressive strength, open porosity, and density were measured. An Instron 3369 testing machine with a maximum load of 50 kN was used for testing. Strength was determined according to ISO 14544:2013, the apparent density according to ISO 787-11, and the open porosity according to ISO 15901-2. Measurements were carried out for 5 samples, and the results were averaged. To study the surface morphology of the obtained ceramic samples and determine the distribution of chemical components, a Hitachi SU3500/Model 3500 electron microscope at an accelerating voltage of 15 kV was utilized. The distribution of elements was assessed using a BRUKER XFlash 6160 energy-dispersive X-ray analyzer and a BRUKER XSense WD waveguide X-ray analyzer. To study the recrystallization processes and the mechanism of nucleation, growth, and destruction of hexagonal inclusions, a Hitachi S-5500 ultra-high-resolution scanning electron microscope at an accelerating voltage of 3 kV was used. The powder diffraction data of the samples for Rietveld analysis were collected at room temperature with a Haoyuan DX-2700BH powder diffractometer, using Cu-Kα radiation and a linear detector. The step size of 2θ was 0.01°, and the counting time was 0.2 s per step. These structures were used as the starting model for Rietveld refinement, which was performed employing TOPAS 4.2. The phase equilibrium was calculated by utilizing the Gibbs potential minimization method [37]. The effect of HF concentration and firing temperature on strength, density, and open porosity was assessed by constructing a second-degree polynomial and by its subsequent analysis. The characteristic appearance of the bundle of aluminum oxide nanofibers used is presented in Figure 1, showing that the nanofiber is an intertwined bundle of individual fibers with a characteristic size of about 10 nm.

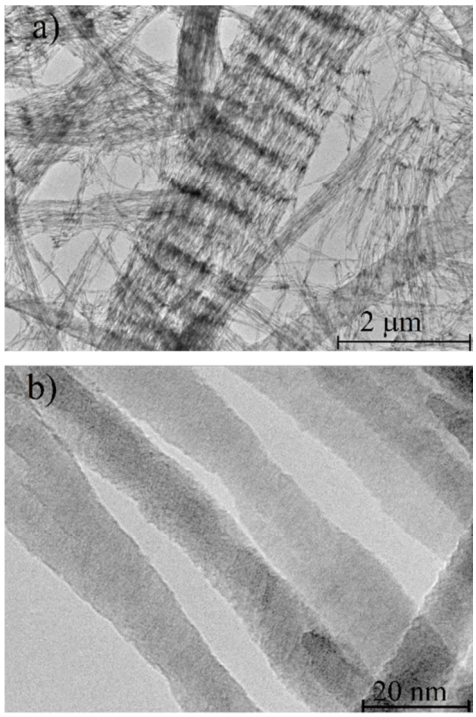

Fig. 1. a) Bundle of nanofibers and b) individual fibers of alumina.

III. PHYSICOCHEMICAL PROCESSES DURING FIRING OF CERAMICS BASED ON ALUMINUM OXIDE NANOFIBERS

When treating γ-Al_2O_3 with HF, two mechanisms of interaction are possible. The first is the formation of AlF_3 on the surface as a result of the chemical reaction (1) [38-40]:

$$Al_2O_3 + HF \rightarrow AlF_3 + H_2O \quad (1)$$

The second is the formation of a substitute solution, in which a Fluorine (F) atom replaces an oxygen atom in the γ-Al_2O_3 crystal structure. This substitution leads to a decrease in the potential barrier for phase transitions and, consequently, to the intensification of ceramic processes in the material. To

assess the direction of chemical development of the system, a phase equilibrium calculation was performed using the Gibbs potential minimization method. The main thermodynamic characteristics are provided in Table I [41].

The results of the thermodynamic calculations are shown in Figure 2. According to the presented data, chemically bound water is completely removed from the γ-Al_2O_3 surface at 400 °C. The resulting AlF_3 completely decomposes at 700 °C. Consequently, the firing start temperature was chosen to be 700 °C. At 1000 °C, the phase transition from γ-Al_2O_3 to κ-Al_2O_3 begins, which leads to the destruction of the fibrous structure. Thus, the maximum firing temperature was set at 1000 °C.

TABLE I. THERMODYNAMIC CHARACTERISTICS OF THE SUBSTANCES UNDER CONSIDERATION [41]

№	Chemical formula	S, [J/mol]	H, [J/mol]	Cp(T)=a+bT10^3+cT^{2}10^{-5}, [J/(mol×K)]
1	Al_2O_3 (α)	50.9	-1675.7	a= 9.76 [J/(mol×K)]; b= 294.7 [J/(mol×K^2)]; c= -2.5 [J/(mol×K^3)]
2	Al_2O_3 (γ)	52.3	-1656.8	a= 119.2 [J/(mol×K)] ; b= 16.9 [J/(mol×K^2)]; c= -37.3 [J/(mol×K^3)]
3	Al_2O_3 (κ)	53.5	-1662.3	a= 116.3 [J/(mol×K)] ; b= 16.5 [J/(mol×K^2)]; c= -36.4 [J/(mol×K^3)]
4	AlF_3	66.5	-1510.4	a= 43.9 [J/(mol×K)] ; b= 128.7 [J/(mol×K^2)]; c= -3.16 [J/(mol×K^3)]
5	HF (g)	173.77	-273.3	a= 29.95 [J/(mol×K)] ; b= -3.14 [J/(mol×K^2)]; c= -0.152 [J/(mol×K^3)]
6	H_2O (g)	188.8	-241.83	a= 28.41 [J/(mol×K)]; b= 12.48 [J/(mol×K^2)]; c=1.28 [J/(mol×K^3)]
7	Al_2O_3* *H_2O	70.67	-1999.1	a= 95.84 [J/(mol×K)] ; b= 34.81 [J/(mol×K^2)];c=-0.034 [J/(mol×K^3)]

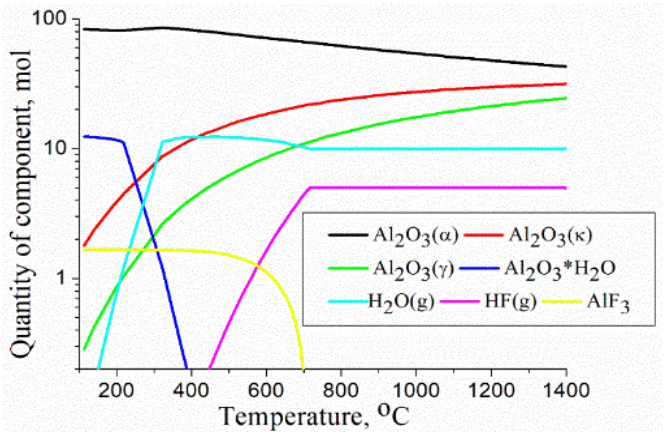

Fig. 2. Results of thermodynamic calculations.

In order to study the phase and chemical changes in the material depending on the firing temperature and HF concentration, X-ray phase analysis was carried out. The results for the components obtained at firing temperatures of 700 °C, 800 °C, 900 °C, and 1000 °C and HF concentrations of 1 % and 3% are displayed in Figure 3.

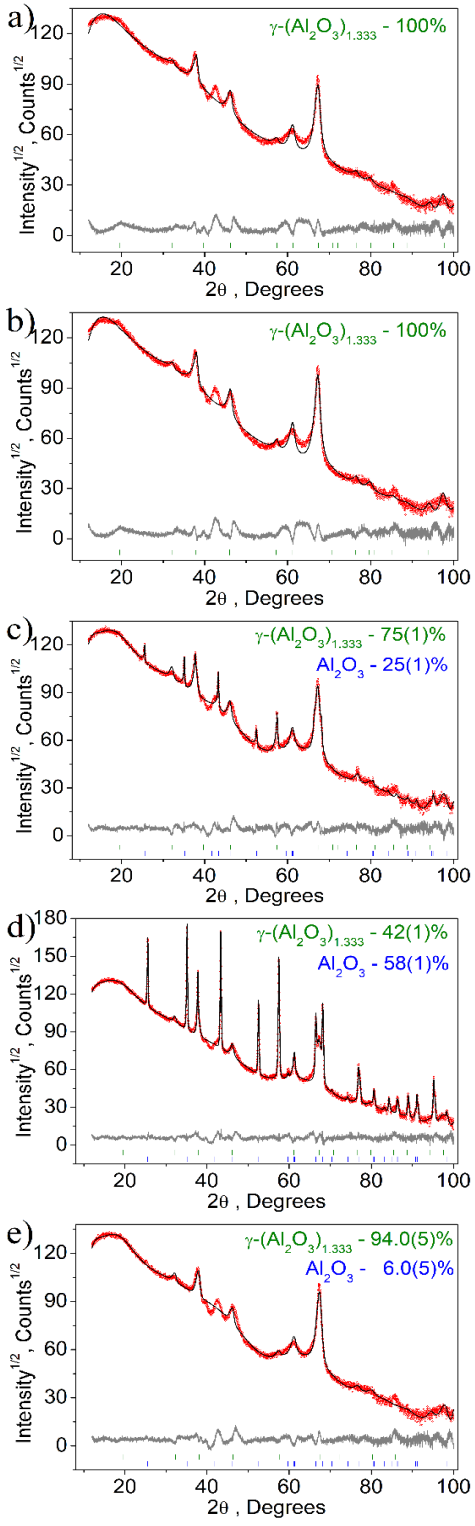

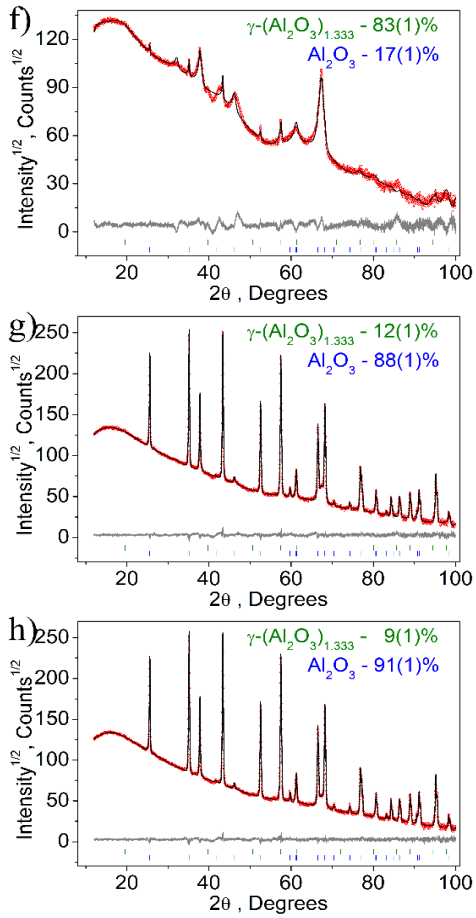

Fig. 3. Results of X-ray phase analysis: obtained at HF concentrations of 1%: a) 700 °C, b) 800 °C, c) 900 °C, d) 1000 °C and at HF concentrations of 3%: e) 700 °C, f) 800 °C, g) 900 °C, h) 1000 °C.

Based on the presented results, the use of HF reduces the phase transition temperature. For 1% HF, the formation of α-Al_2O_3 begins at a temperature of 900 °C, as illustrated in Figure 2c, while the quantitative ratio of α-Al_2O_3 increases at a temperature of 1000 °C, as portrayed in Figure 2d. Increasing the concentration of HF to 3% reduces the phase transition onset temperature to 700 °C, as shown in Figure 3e, and, consequently, the amount of α-Al_2O_3 in the material obtained at a concentration of 3% HF is greater than at a concentration of 1%. The absence of peaks characteristic of AlF_3 indicates its/the latter's complete decomposition during the firing process. At the same time, with the formation of the α-form, a decrease in the width of the spectra is observed, which exhibits the formation of larger crystallites.

IV. STUDY OF THE MORPHOLOGY OF THE CHIP SURFACE OF A SAMPLE AFTER DESTRUCTION

Based on the X-ray phase analysis, shown in Figure 3, the γ-$Al_2O_3 \rightarrow$ α-Al_2O_3 phase transition occurs during the firing process. In this case, the crystal lattice changes from tetragonal (a=b=0.562 nm, c=0.780 nm) of the spinel type, with a density of 3.3-3.4 g/cm³ for γ-Al_2O_3, to hexagonal (a=b=0.475 nm, c=1.299 nm), with a density of 3.99 g/cm³ for α-Al_2O_3. This leads to the destruction of the fibrous structure and the formation of hexagonal plates. Microphotographs of the samples with an HF concentration of 1%, obtained at temperatures of 700 °C, 800 °C, 900 °C, and 1000 °C, at 50,000 times magnification, are displayed in Figure 4. Microphotographs for samples with HF concentrations of 3% obtained at temperatures of 700 °C, 800 °C, 900 °C, and 1000 °C, at 50,000 times magnification, are portrayed in Figure 5.

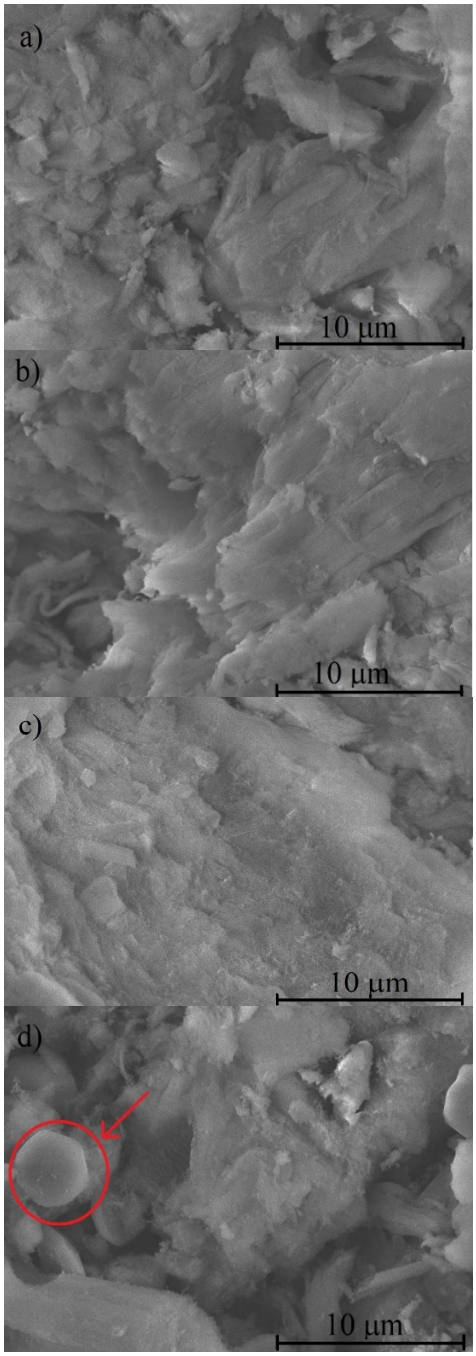

Fig. 4. Micrographs obtained at 1% HF concentrations: a) 700 °C, b) 800 °C, c) 900 °C, d) 1000 °C.

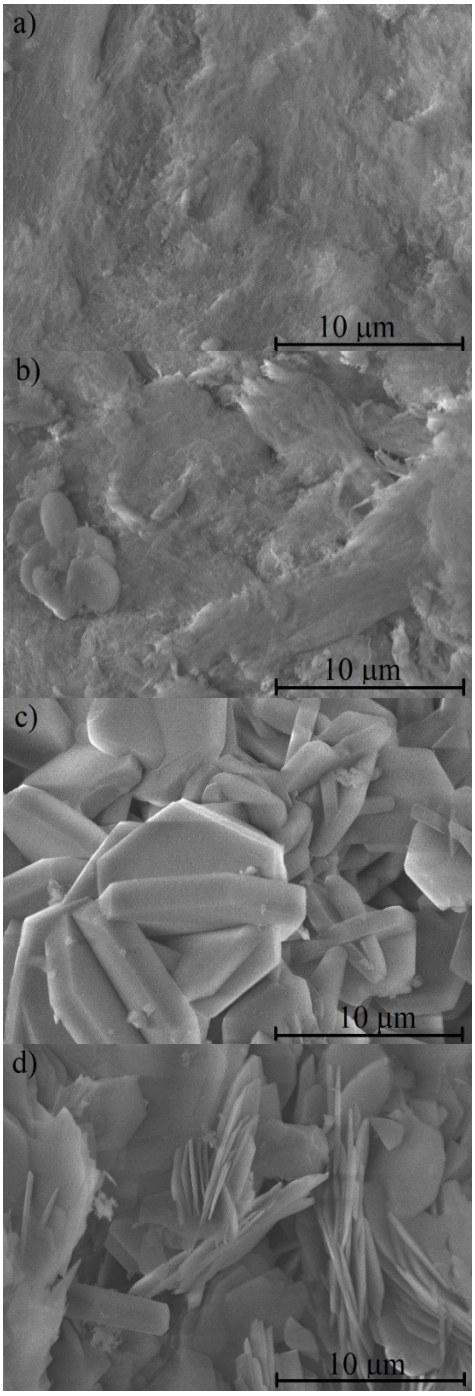

Fig. 5. Micrographs obtained at HF concentrations of 3%: a) 700 °C, b) 800 °C, c) 900 °C, d) 1000 °C.

The fibrous structure is retained for the ceramics in the γ-form, as evidenced in Figure 4(a-b). When α-Al_2O_3 begins to predominate in the material, hexagonal plates are formed. Consequently, the destruction of the fibrous structure occurs in several stages. First, amorphous conglomerates are formed, which gradually transform into hexagonal plates. For the ceramics obtained at a temperature of 1000 °C and a concentration of 3% HF, delamination of the plates is observed.

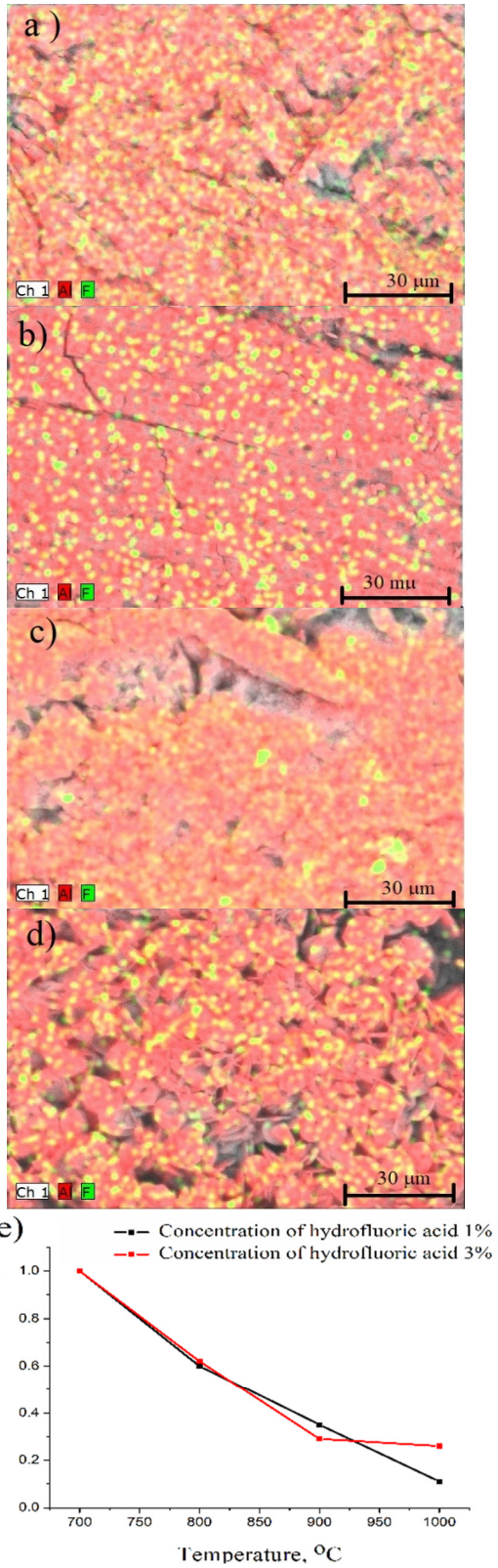

Fig. 6. Results of X-ray fluorescence analysis for HF concentration of a) 1% at 700 °C and b) at 1000 °C, c) HF concentration of 3% at 700 °C and d) at 1000 °C, and e) the integral value of the number of F atoms from the firing temperature.

To assess the distribution of F atoms in the lattice, the results of X-ray fluorescence analysis are presented for the material obtained at HF concentrations of 1% and 3% at firing temperatures ranging from 700 °C to 1000 °C. The integral value of the number of F atoms as a function of temperature, normalized by the concentration at 700 °C, is illustrated in Figure 6. Based on Figure 6, with increasing temperature, the concentration of F atoms in the crystal lattice decreases linearly. This is validated by the straight lines coinciding in Figure 6e. Moreover, at an HF concentration of 3%, there were approximately twice as many F atoms compared to 1% HF. It also appears that F is incorporated into the crystalline lattice of Al_2O_3 as a substitutional solution.

V. STUDY OF THE PROCESS OF ORIGIN, DEVELOPMENT AND DESTRUCTION OF HEXAGONAL STRUCTURES

The formation and development of hexagonal inclusions in the material significantly influences its physico-mechanical properties. This process was investigated with high-resolution micrographs obtained for temperatures of 700 °C, 800 °C, 900 °C, and 1000 °C, and HF concentrations of 1% and 3%, as presented in Figure 7.

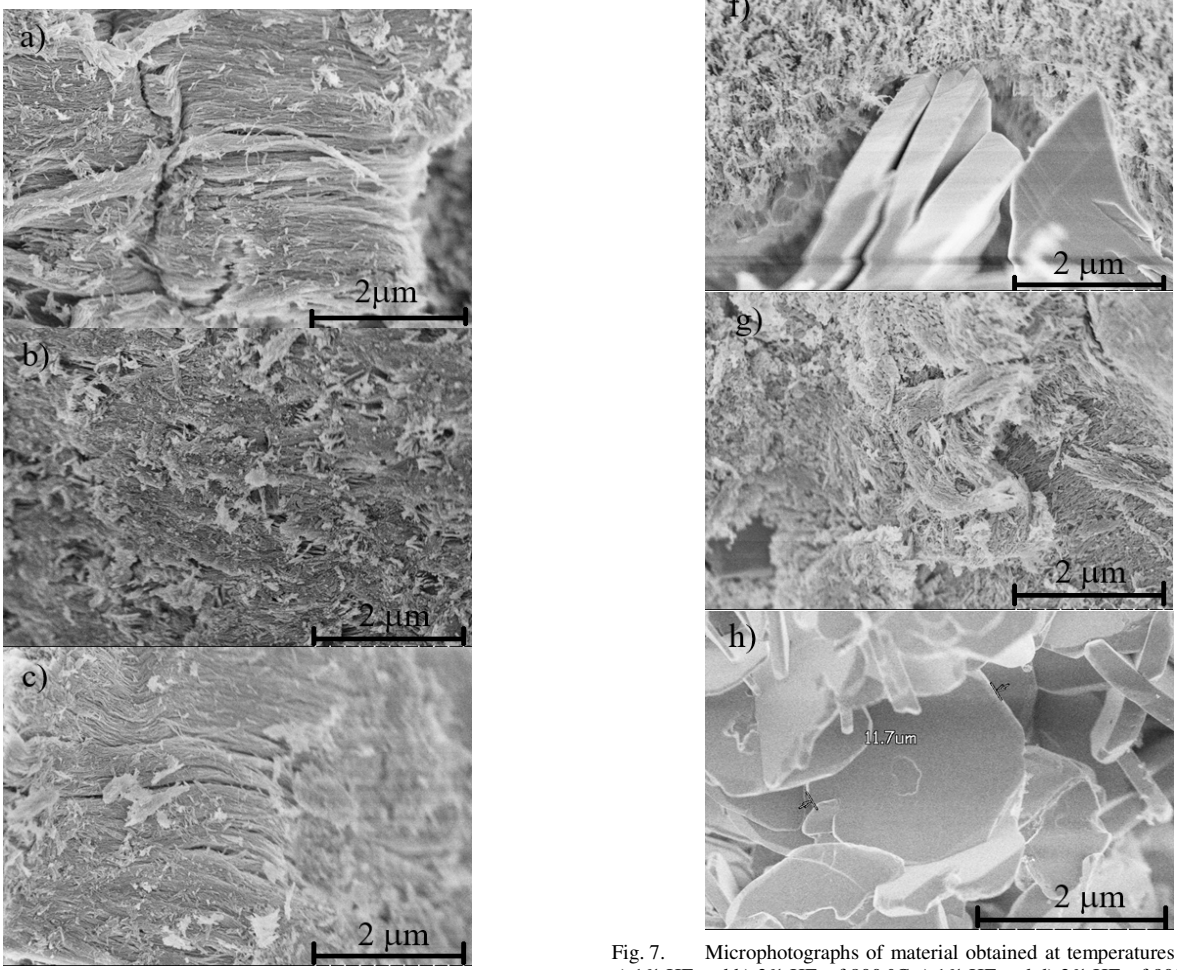

Fig. 7. Microphotographs of material obtained at temperatures of 700 °C a) 1% HF and b) 3% HF, of 800 °C c) 1% HF and d) 3% HF, of 900 °C e) 1% HF and f) 3% HF, and of 1000 °C g) 1% HF and h) 3% HF.

For the material pre-treated with a 1% HF solution, the fibrous structure is preserved within the temperature range of 700-800 °C. At temperatures of 900 °C and 1000 °C, the formation of conglomerates is observed, but the decrease in the potential barrier is insufficient for the formation of hexagonal plates. Therefore, the number of F atoms at this concentration of HF is insufficient for significant activation of the γ-$Al_2O_3 \rightarrow \alpha$-$Al_2O_3$ phase transition, so this transition occurs at a lower rate. At a temperature of 700 °C, an insignificant amount of the α-phase is observed for the material obtained with 3% HF. The results obtained at a temperature of 1000 °C and a concentration of 1% HF, as depicted in Figure 7g, are comparable with the results at a temperature of 700 °C and a concentration of 3% HF, demonstrated in Figure 7b. In general, the fibrous structure is preserved at a concentration of 1% HF. Hexagonal structures are formed at a certain number of F atoms in the crystal lattice of Al_2O_3. The formation of hexagonal plates occurs in several stages. In the first stage, amorphous structures begin to form, as illustrated in Figure 7b, and in the second stage, these structures gradually transform into cubic conglomerates, as evidenced in Figure 7d. In the third stage, plates begin to grow from the conglomerates, as displayed in Figure 7f. At a temperature of 1000 °C and an HF concentration of 3%, virtually all fibrous Al_2O_3 is transformed into plates. In this case, the presence of γ-Al_2O_3 is not observed, which indicates that these plates represent the α-form.

VI. PHYSICAL AND MECHANICAL PROPERTIES OF CERAMIC MATERIALS

The quality of sintering of ceramic materials can be determined by physical and mechanical characteristics: density, strength, and open porosity. The dependence of density, strength, and open porosity on the firing temperature for a ceramic material based on Al_2O_3 nanofiber obtained at different concentrations of HF are shown in Figure 8, as well as the dependence of strength on density.

Based on Figure 8, the optimal concentration of HF, allowing for the best indicators of strength, density, and open porosity, is 1%. At this concentration, the fibrous structure of the material is preserved, as can be seen in Figure 4. The optimal firing temperature is 800 °C. This temperature is insufficient for significant activation of the phase transition from γ to α. However, the diffusion of F atoms in the crystal lattice of Al_2O_3 begins, which promotes sintering and, consequently, an increase in the physical and mechanical properties of the material. Increasing the concentration of HF to 3% activates the phase transition $\gamma \rightarrow \alpha$, leading to a decrease in the physical and mechanical properties. Proof of this is provided by the results of XRF analysis and the microphotographs obtained, as presented in Figure 6. According to the semi-quantitative analysis data, the amount of α-Al_2O_3 is 17% for the material obtained with a concentration of 3% HF at a firing temperature of 800 °C, as illustrated in Figure 3f. At the same time, hexagonal conglomerates were found in the microphotographs in Figures 4 and 5. The temperature of 700 °C is insufficient to initiate active diffusion of F atoms in the system. The dependence of strength on porosity is shown in Figure 8d. It is demonstrated that the material obtained with a concentration of 1% HF is best sintered. This is exhibited by the maximum angle of 69° in the presented dependence. The optimal physical and mechanical characteristics are a compressive strength of 49 MPa with a porosity of 46% and a density of 1.47 g/cm³. To assess the influence of temperature and HF concentration, a second-degree polynomial was constructed using these two as variables. The results are shown in Figure 9.

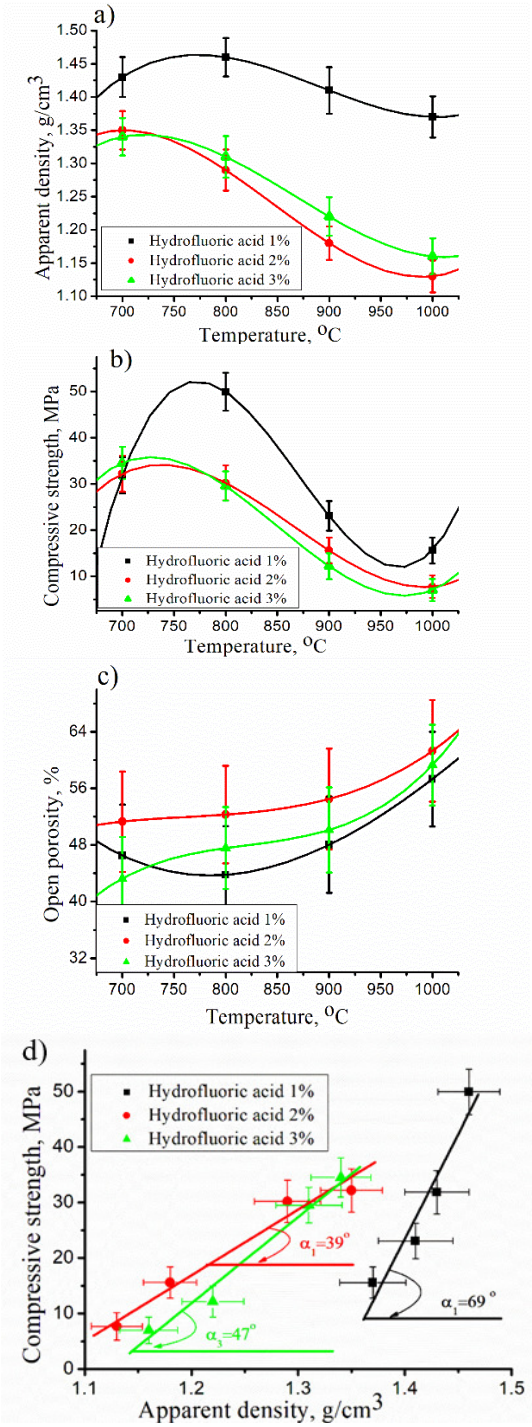

Fig. 8. Dependence of a) density, b) strength, c) open porosity on the firing temperature, and d) dependence of strength on density.

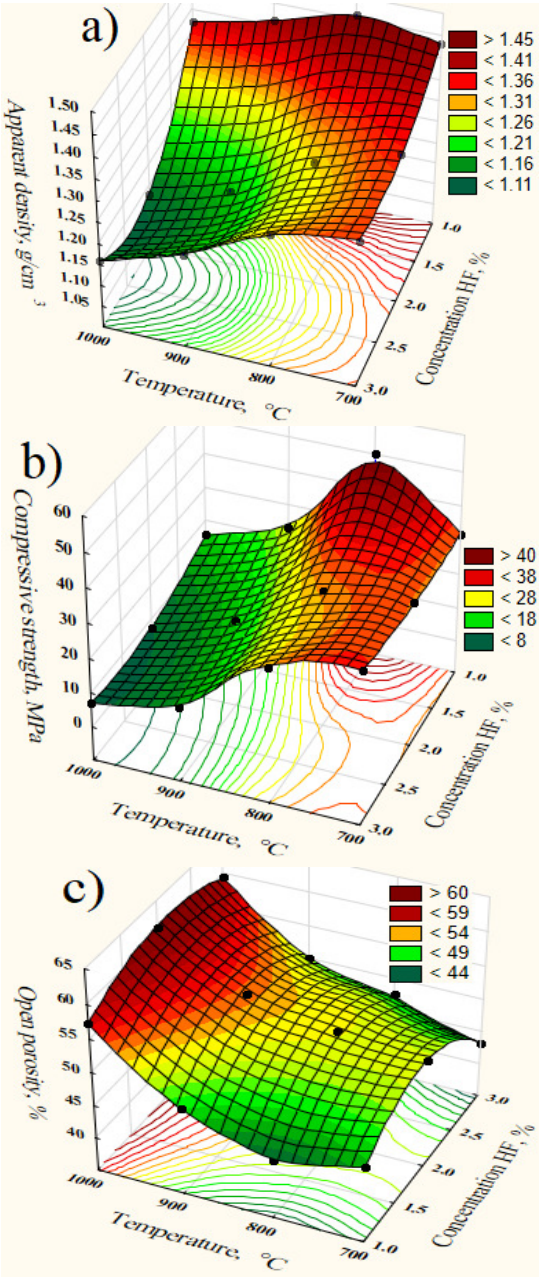

Fig. 9. Graphical representation of the constructed polynomial: a) for density, b) for strength, and c) for open porosity.

In this work, ceramics based on aluminum nanofibers with diameters of approximately 5-10 nm and a high aspect ratio (>1000) were obtained and investigated after treatment with HF. Ceramics using HF from this fiber were obtained for the first time. The influence of HF on the γ to α phase transition for this nanofiber was studied. The use of HF leads to a significant reduction in the phase transition temperature (down to 800 °C). As a result of this phase transition, the fibrous structure is destroyed, leading to the formation of hexagonal-shaped plates. This results in a decrease in strength and density, as well as an increase in the porosity of the obtained materials.

VII. CONCLUSION

When treating γ-Al_2O_3 with Hydrofluoric Acid (HF), two interaction mechanisms were revealed. The first mechanism involves the formation of AlF_3 on the surface of the material. The second mechanism is associated with the replacement of oxygen with Fluorine (F) atoms in the γ-Al_2O_3 crystal lattice, which reduces the potential barrier for phase transitions and accelerates ceramic processes. Thermodynamic calculations showed that AlF_3 decomposes at 700 °C, which became the temperature at which the ceramic material begins to synthesize. The phase transition from γ-Al_2O_3 to α-Al_2O_3 begins at 900 °C for 1% HF, and at 700 °C for 3% HF. The morphology study showed that the fibrous structure is preserved in the γ-form and is destroyed during the phase transition. An increase in the HF concentration leads to the formation of hexagonal plates that destroy the fibrous structure, which reduces the physical and mechanical properties of the material. The optimal concentration of HF to achieve the best physical and mechanical properties is 1% at a firing temperature of 800 °C, since this is the maximum temperature at which the fibrous structure of the material is preserved. The optimal physical and mechanical characteristics are a compressive strength of 49 MPa with a porosity of 46% and a density of 1.47 g/cm³. An increase in temperature and HF concentration activates the phase transition, which negatively affects the strength and density of the material.

ACKNOWLEDGMENT

Electron microscopy measurements were performed on the equipment of Krasnoyarsk Regional Center of Research Equipment of Federal Research Center "Krasnoyarsk Science Center SB RAS". The work was carried out within the state assignment No. FWES-2024-0026 of Federal Research Center "Krasnoyarsk Science Center of the Siberian Branch of the Russian Academy of Sciences."

REFERENCES

[1] P. Baldus, M. Jansen, and D. Sporn, "Ceramic Fibers for Matrix Composites in High-Temperature Engine Applications," *Science*, vol. 285, no. 5428, pp. 699–703, Jul. 1999, https://doi.org/10.1126/science.285.5428.699.

[2] D. J. Pysher, K. C. Goretta, R. S. Hodder, and R. E. Tressler, "Strengths of Ceramic Fibers at Elevated Temperatures," *Journal of the American Ceramic Society*, vol. 72, no. 2, pp. 284–288, Feb. 1989, https://doi.org/10.1111/j.1151-2916.1989.tb06115.x.

[3] Z. Xu *et al.*, "A review of the research progress on the interface between oxide fiber and oxide ceramic matrix," *Ceramics International*, vol. 47, no. 5, pp. 5896–5908, Mar. 2021, https://doi.org/10.1016/j.ceramint.2020.11.039.

[4] S. Wang *et al.*, "Integrated process for membrane fouling mitigation and organic pollutants removal using copper oxide modified ceramic hollow fiber membrane with in-situ peroxymonosulfate activation," *Chemical Engineering Journal*, vol. 396, Sep. 2020, Art. no. 125289, https://doi.org/10.1016/j.cej.2020.125289.

[5] P. Colomban and G. Gouadec, "The ideal ceramic-fibre/oxide-matrix composite: how to reconcile antagonist physical and chemical requirements?," *Annales de Chimie Science des Matériaux*, vol. 30, no. 6, pp. 673–688, Dec. 2005, https://doi.org/10.3166/acsm.30.673-688.

[6] X. Dong *et al.*, "Synthesis and properties of lightweight fibrous ceramics with a 3D skeleton structure prepared by infiltration," *Materials Science and Engineering: A*, vol. 635, pp. 43–49, May 2015, https://doi.org/10.1016/j.msea.2015.03.062.

[7] N. Zhou *et al.*, "Lightweight quasi-layered elastic fibrous porous ceramics with high compressive stress and low thermal conductivity," *Journal of Materials Science & Technology*, vol. 143, pp. 207–215, Apr. 2023, https://doi.org/10.1016/j.jmst.2022.09.047.

[8] J. Zhang, X. Dong, F. Hou, H. Du, J. Liu, and A. Guo, "Effects of fiber length and solid loading on the properties of lightweight elastic mullite fibrous ceramics," *Ceramics International*, vol. 42, no. 4, pp. 5018–5023, Mar. 2016, https://doi.org/10.1016/j.ceramint.2015.11.176.

[9] G. Zhao, L. Shi, G. Yang, X. Zhuang, and B. Cheng, "3D fibrous aerogels from 1D polymer nanofibers for energy and environmental applications," *Journal of Materials Chemistry A*, vol. 11, no. 2, pp. 512–547, 2023, https://doi.org/10.1039/D2TA05984C.

[10] C. Jia, Z. Xu, D. Luo, H. Xiang, and M. Zhu, "Flexible Ceramic Fibers: Recent Development in Preparation and Application," *Advanced Fiber Materials*, vol. 4, no. 4, pp. 573–603, Aug. 2022, https://doi.org/10.1007/s42765-022-00133-y.

[11] X. Lu and M. Viljanen, "Fibrous insulation materials in building engineering applications," in *Fibrous and Composite Materials for Civil Engineering Applications*, Elsevier, 2011, pp. 271–305.

[12] T. E. Steyer, "Shaping the Future of Ceramics for Aerospace Applications," *International Journal of Applied Ceramic Technology*, vol. 10, no. 3, pp. 389–394, May 2013, https://doi.org/10.1111/ijac.12069.

[13] W. O. Soboyejo, J. D. Obayemi, E. Annan, E. K. Ampaw, L. Daniels, and N. Rahbar, "Review of High Temperature Ceramics for Aerospace Applications," *Advanced Materials Research*, vol. 1132, pp. 385–407, Dec. 2015, https://doi.org/10.4028/www.scientific.net/AMR.1132.385.

[14] L. Miao, Z. Ji, X. Wang, and X. Wu, "Insights into the calcination temperature and loading amount of the catalyst support (TiO2) in the fibrous ceramic-based catalytic filter element prepared by microwave drying," *Ceramics International*, vol. 49, no. 19, pp. 31057–31065, Oct. 2023, https://doi.org/10.1016/j.ceramint.2023.07.050.

[15] C. Voigt *et al.*, "Filtration Efficiency of Functionalized Ceramic Foam Filters for Aluminum Melt Filtration," *Metallurgical and Materials Transactions B*, vol. 48, no. 1, pp. 497–505, Feb. 2017, https://doi.org/10.1007/s11663-016-0869-5.

[16] S. Tang and C. Hu, "Design, Preparation and Properties of Carbon Fiber Reinforced Ultra-High Temperature Ceramic Composites for Aerospace Applications: A Review," *Journal of Materials Science & Technology*, vol. 33, no. 2, pp. 117–130, Feb. 2017, https://doi.org/10.1016/j.jmst.2016.08.004.

[17] B. Saruhan, Oxide-Based Fiber-Reinforced Ceramic-Matrix Composites. Boston, MA: Springer US, 2003.

[18] C. G. Aneziris and H. Biermann, Eds., *Multifunctional Ceramic Filter Systems for Metal Melt Filtration: Towards Zero-Defect Materials*, vol. 337. Cham: Springer International Publishing, 2024.

[19] V. S. Solodovnichenko *et al.*, "Coupled thermal analysis of carbon layers deposited on alumina nanofibres," *Thermochimica Acta*, vol. 675, pp. 164–171, May 2019, https://doi.org/10.1016/j.tca.2019.02.012.

[20] I. A. Kharchenko *et al.*, "Enhancement of ionic conductivity in electrically conductive membranes by polarization effect," *Electrochimica Acta*, vol. 506, Dec. 2024, Art. no. 144994, https://doi.org/10.1016/j.electacta.2024.144994.

[21] K. Boukerma and M. Kadja, "Convective Heat Transfer of Al2O3 and CuO Nanofluids Using Various Mixtures of Water-Ethylene Glycol as Base Fluids," *Engineering, Technology & Applied Science Research*, vol. 7, no. 2, pp. 1496–1503, Apr. 2017, https://doi.org/10.48084/etasr.1051.

[22] J. Zhu, R. Zhu, Y. Hu, and Z. Wang, "Mullite fiber porous ceramic with high quality factor for high-temperature PM filtration," *Journal of the European Ceramic Society*, vol. 44, no. 4, pp. 2630–2637, Apr. 2024, https://doi.org/10.1016/j.jeurceramsoc.2023.11.064.

[23] E. S. Hevorkian, V. P. Nerubatskyi, R. V. Vovk, T. Szumiata, and J. N. Latosińska, "Foamy ceramic filters and new possibilities of their applications," *Ceramics International*, vol. 50, no. 4, pp. 6961–6968, Feb. 2024, https://doi.org/10.1016/j.ceramint.2023.12.046.

[24] R. A. Venis and O. D. Basu, "Mechanisms and efficacy of disinfection in ceramic water filters: A critical review," *Critical Reviews in Environmental Science and Technology*, vol. 51, no. 24, pp. 2934–2974, Dec. 2021, https://doi.org/10.1080/10643389.2020.1806685.

[25] H. O. Mohamed *et al.*, "Isolating the effect of Co and Ce on Ni–X–Y/Al2O3 bi- and trimetallic reforming catalysts for hydrogen generation," *International Journal of Hydrogen Energy*, vol. 51, pp. 922–935, Jan. 2024, https://doi.org/10.1016/j.ijhydene.2023.10.257.

[26] N. A. Zhirov, A. S. Akimov, Y. E. Barbashin, and A. S. Akimov, "Texture Properties, Phase Composition and Morphology of Supported Ni-Mo /γ- Al2O3 Systems," *Journal of Siberian Federal University*, vol. 16, no. 4, pp. 477–484, Oct. 2023.

[27] A. S. Noskov, "Synthesis and application of inorganic oxide materials for oil hydroprocessing catalysts," *Russian Chemical Bulletin*, vol. 72, no. 2, pp. 367–378, Feb. 2023, https://doi.org/10.1007/s11172-023-3805-5.

[28] I. Aziz, P. Sugita, N. Darmawan, and A. A. Dwiatmoko, "Synthesis of Green Diesel from Palm Oil Using Nickel-based Catalyst: A Review," *Jurnal Kimia Valensi*, vol. 9, no. 1, pp. 59–75, May 2023, https://doi.org/10.15408/jkv.v9i1.26488.

[29] B. Abrar, M. Halali, and A. Pourfathi, "Recovery of Nickel from Reformer Catalysts of Direct Reduction, Using the Pressurized Dissolving Method in Nitric Acid," *Engineering, Technology & Applied Science Research*, vol. 6, no. 5, pp. 1158–1161, Oct. 2016, https://doi.org/10.48084/etasr.731.

[30] A. Z. Al-Khazaal, F. Ahmad, and N. Ahmad, "Study on the Removal of Thiosulfate from Wastewater by Catalytic Oxidation," *Engineering, Technology & Applied Science Research*, vol. 9, no. 2, pp. 4053–4056, Apr. 2019, https://doi.org/10.48084/etasr.2553.

[31] A. G. Olaremu, "Preparation and characterization of CoMo catalyst supported on organized mesoporous zeolite from Kaolin clay," *Journal of Medicinal and Nanomaterials Chemistry*, vol. 6, no. 2, Jun. 2024, https://doi.org/10.48309/jmnc.2024.2.4.

[32] Y. Chen, N. Wang, O. Ola, Y. Xia, and Y. Zhu, "Porous ceramics: Light in weight but heavy in energy and environment technologies," *Materials Science and Engineering: R: Reports*, vol. 143, Jan. 2021, Art. no. 100589, https://doi.org/10.1016/j.mser.2020.100589.

[33] A. V. Minakov *et al.*, "Rheological properties of colloidal suspensions of alumina nanofibers," *Journal of Molecular Liquids*, vol. 367, Dec. 2022, Art. no. 120385, https://doi.org/10.1016/j.molliq.2022.120385.

[34] S. S. Dobrosmyslov et al., "Investigation of the Effect of Nanoscale Alumina Fiber on the Heat Resistance of Refractory Concrete," *Refractories and Industrial Ceramics*, vol. 61, no. 6, pp. 704–708, Mar. 2021, https://doi.org/10.1007/s11148-021-00546-z.

[35] S. Peng *et al.*, "Effect of halide mineralizers on monodisperse spherical zircon powders," *Journal of the American Ceramic Society*, vol. 104, no. 6, pp. 2849–2859, Jun. 2021, https://doi.org/10.1111/jace.17636.

[36] V. Gurieva and A. V. Doroshin, "The Press Powder Technological Parameters Optimization in Wall Ceramics Production by the Semi-Dry Pressing Method," *Materials Science Forum*, vol. 974, pp. 419–423, Dec. 2019, https://doi.org/10.4028/www.scientific.net/MSF.974.419.

[37] S. S. Dobrosmyslov, A. S. Voronin, Y. V. Fadeev, I. G. Endzhievskaya, and S. V. Khartov, "Theoretical and experimental study of the effect of wollastonite on the physical and mechanical properties of concrete," *Journal of Physics: Conference Series*, vol. 2094, no. 2, Nov. 2021, Art. no. 022077, https://doi.org/10.1088/1742-6596/2094/2/022077.

[38] L. N. W. Damoah and L. Zhang, "AlF3 reactive Al2O3 foam filter for the removal of dissolved impurities from molten aluminum: Preliminary results," *Acta Materialia*, vol. 59, no. 3, pp. 896–913, Feb. 2011, https://doi.org/10.1016/j.actamat.2010.09.064.

[39] Y. Lee, J. W. DuMont, and S. M. George, "Mechanism of Thermal Al2O3 Atomic Layer Etching Using Sequential Reactions with Sn(acac)2 and HF," *Chemistry of Materials*, vol. 27, no. 10, pp. 3648–3657, May 2015, https://doi.org/10.1021/acs.chemmater.5b00300.

[40] X. Delong, L. Yongqin, J. Ying, Z. Longbao, and G. Wenkui, "Thermal behavior of aluminum fluoride trihydrate," *Thermochimica Acta*, vol. 352–353, pp. 47–52, Jul. 2000, https://doi.org/10.1016/S0040-6031(99)00436-0.

[41] I. Barin, *Thermochemical Data of Pure Substances*, Third edition. Weinheim: VCH Verlagsgesellschaft mbH, 2008.